JOURNAL OF GEOPHYSICAL RESEARCH, VOL. 100, NO. D7, PAGES 14,175–14,188, JULY 20, 1995

The use of NO_y, H_2O_2, and HNO_3 as indicators for ozone-NO_x-hydrocarbon sensitivity in urban locations

Sanford Sillman

Department of Atmospheric, Oceanic, and Space Sciences, University of Michigan, Ann Arbor

Abstract. Correlations are presented between model predictions for O_3-NO_x-hydrocarbon sensitivity and afternoon concentrations of four "indicator species": NO_y, $O_3/(NO_y - NO_x)$, $HCHO/NO_y$, and H_2O_2/HNO_3. The indicator species correlations are based on a series of photochemical simulations with varying rates of anthropogenic and biogenic emissions and meteorology. Hydrocarbon-sensitive chemistry in models is shown to be linked to afternoon NO_y > 20 ppb, $O_3/(NO_y - NO_x) < 7$, $HCHO/NO_y < 0.28$, and $H_2O_2/HNO_3 < 0.4$. Lower NO_y and higher ratios correspond with NO_x-sensitive ozone. The correlation between NO_x-hydrocarbon sensitivity and indicator species remains, even when model emission rates and hydrocarbon/NO_x ratios are changed by a factor of 2. Methods are developed for evaluating the goodness of fit between model NO_x-hydrocarbon sensitivity and indicator values. Ozone chemistry is also analyzed in terms of fundamental properties of odd hydrogen, and theoretical criteria for the transition between NO_x- and hydrocarbon-sensitive regimes are derived. A theoretical correlation between O_3 and $H_2O_2 + NO_y - NO_x$ is developed as a way to extend rural O_3-NO_y correlations into urban locations. Measured indicator values during pollution events in Los Angeles, Atlanta, and rural Virginia are used to illustrate the range of observed values under different environmental conditions.

Introduction

The relationship among ozone, NO_x, and reactive organic gases (ROG) in polluted environments represents a major uncertainty in terms of both science and public policy. It is generally known that for certain conditions the rate of ozone formation will increase with increasing NO_x and will be insensitive to ROG, while for other conditions the rate of formation will increase with increasing ROG and will be unchanged (or perhaps even decrease) with increasing NO_x. However, the question of whether peak ozone concentrations in a specific location are sensitive to NO_x or to ROG has proven elusive.

A major problem for the study of ozone-NO_x-ROG sensitivity has been the inability to gain evidence based on direct measurements rather than theoretical calculations. Evaluations of ozone-NO_x-ROG sensitivity have relied on results of three-dimensional dynamical/photochemical models such as the Urban Airshed Model (UAM). These evaluations are difficult because they depend on assumptions, e.g., about emission rates, that are highly uncertain [*Fujita et al.*, 1992] and because predicted sensitivity cannot be tested empirically. Model accuracy is assessed by comparing predicted and observed ozone and occasionally other species [*Tesche et al.*, 1990]. Even when the model application appears successful in comparison with measured ozone there may still be considerable doubt about the accuracy of the model prediction for ozone-NO_x-ROG sensitivity. Because similar quantities of ozone can be produced in ROG-sensitive and NO_x-sensitive environments, it is possible for a simulation to return accurate predictions for ozone and still err in its prediction for sensitivity. In recent years, model assessment has been improved by including comparisons with measured concentrations of primary ROG species [*Tesche et al.*, 1990]. Since primary species concentrations are strongly affected by micrometeorology, vertical mixing rates, and on-site sources, there is still room for doubt concerning model sensitivity predictions.

An alternative approach to determining ozone sensitivity is to identify individual species or species ratios that consistently assume different values under conditions of NO_x-sensitive and ROG-sensitive ozone. If these types of "indicator species" can be identified, then ozone-NO_x-ROG sensitivity could be determined directly from measurements rather than from models. Comparisons between model predictions and measured values for the indicator species would also provide a test of the accuracy of model sensitivity predictions.

Milford et al. [1994] have established a link between ozone, sensitivity and total reactive nitrogen (NO_y=NO_x + HNO_3 + peroxyacetylnitrates + alkyl nitrates). In the study by *Milford et al.*, low values of afternoon NO_y (<12 ppb) were consistently associated with NO_x-sensitive ozone, and high values of NO_y (>25 ppb) were associated with ROG-sensitive ozone, based on sensitivity predictions from four different model applications to cities and regions in the United States. The potential link between sensitivity and NO_x demonstrated by *Milford et al.* [1994] is especially useful because laboratory techniques for measurement of NO_y have been extensively developed, tested, and applied [*Trainer et al.*, 1993; *Fehsenfeld et al.*, 1987].

The indicator species approach to ozone sensitivity has two significant drawbacks. First, correlations between sensitivity and indicator species (e.g., NO_y) may shift significantly when changes in initial emission rates are made. This type of shift would suggest that the indicator-based estimates for ozone

Paper number 94JD02953.
0148-0227/95/94JD-02953$05.00

sensitivity still depend on model assumptions rather than provide a fully independent estimate. Second, the theoretical results that link ozone sensitivity with an indicator species provide no basis for testing the validity of the theory. Whereas the original determination of sensitivity through photochemical modeling required an essentially untestable faith in the accuracy of model ozone-NO_x-ROG sensitivity, the use of indicator species such as NO_y appears to require a similarly untestable faith in the accuracy of the model-based indicator species correlation.

This paper extends the indicator-species concept of *Milford et al.* [1994] to include three additional empirical indicators for NO_x-sensitive versus ROG-sensitive ozone: the ratios $O_3/(NO_y - NO_x)$, $HCHO/NO_y$, and H_2O_2/HNO_3 (or H_2O_2/NO_y). Along with NO_y, these species provide four semi-independent indicators for ozone sensitivity. The $HCHO/NO_y$ and H_2O_2/HNO_3 ratios involve species that are more difficult to measure than NO_y, but measurement techniques exist [*Kleindeinst et al.*, 1988; *Hering et al.*, 1988; *Lee et al.*, 1993, 1994], and they provide a link with ozone sensitivity that relates to model assumptions in a different way than NO_y does. In addition, the identification of four separate indicators for ozone sensitivity provides for a more rigorous evaluation because the individual indicators must be consistent with one another. This provides for a limited validation of the theory through a comparison of simulated and observed correlations between the species. Sensitivity correlations and correlations between indicator species are shown for photochemical model applications to the Lake Michigan region and the northeast corridor of the United States. [*Sillman et al.*, 1993] with a wide range of initial assumptions. Measurements during air pollution events in Los Angeles, Atlanta, and rural Virginia show that the indicator species assume different values in different photochemical environments.

Overview of Relevant Chemistry

Although the chemistry of urban ozone formation is well known [e.g., National Research Council (NRC), 1991], some aspects of chemistry that relate to ozone sensitivity and the indicator species are not well known and are worth summarizing. The ozone-producing reaction sequence is almost always initiated by the reaction of a hydrocarbon with OH,

$$\text{(R1)} \qquad RH + OH \xrightarrow{[O_2]} RO_2 + H_2O$$

followed by reactions of RO_2 and HO_2 radicals with NO,

$$\text{(R2)} \qquad RO_2 + NO \xrightarrow{[O_2]} R'CHO + HO_2 + NO_2$$

$$\text{(R3)} \qquad HO_2 + NO \xrightarrow{[O_2]} OH + NO_2$$

(For example, propane (C_3H_8) reacts via (R1) to form the RO_2 radical $C_3H_7O_2$ and then via (R2) to form propionaldehyde (C_2H_5CHO). Most hydrocarbons have more complex reaction pathways, but the general pattern of RH to RO_2 via (R1) and to an intermediate carbonyl via (R2) accounts for most hydrocarbon reactions.)

The conversion of NO to NO_2 results in the production of an ozone following photolysis of NO_2. Since the radical reactions occur rapidly, the hydrocarbon-OH reaction represents the rate-limiting step for the sequence. The intermediate aldehyde product R'CHO (replaced by a ketone or dicarbonyl for many hydrocarbon species) may undergo further ozone-producing reactions, initiated either by reaction with OH or by photolysis.

At moderately high NO_x concentrations ($NO_x > 0.3$ ppb), reactions (R2) and (R3) represent the dominant reaction pathway for RO_2 and HO_2 radicals, and ozone production rates are roughly proportional to reaction (R1). Consequently, the rate of ozone production is roughly proportional to the summed rate of the hydrocarbon + OH reactions (R1) along with the analogous reaction with CO,

$$\text{(R4)} \qquad CO + OH \xrightarrow{[O_2]} HO_2 + CO_2$$

In most urban environments and in the polluted rural environments of Europe and the eastern United States there is an abundant supply of NO_x, CO, and hydrocarbons to fuel the ozone-producing reactions. The rate of ozone production and the division into NO_x-sensitive and ROG-sensitive photochemical regimes is linked to the abundance of the OH radical and the odd hydrogen cycle.

Odd hydrogen in polluted environments is most conveniently viewed as the sum of OH, HO_2, and RO_2 radicals rather than simply OH + HO_2 [*Kleinman*, 1986, 1991; *Sillman et al.*, 1990b; *Sillman*, 1991]. With this definition, odd hydrogen is conserved by reactions (R1)-(R4), which also provide the major pathways for interconversion of OH, HO_2, and RO_2. The major sources of odd hydrogen are the photolysis of ozone and subsequent reaction of $O(^1D)$ with water vapor and the photolysis of aldehydes and other intermediate ROG species. The important sinks of odd hydrogen are

$$\text{(R5)} \qquad HO_2 + HO_2 \rightarrow H_2O_2 + O_2$$

$$\text{(R6)} \qquad RO_2 + HO_2 \rightarrow ROOH + O_2$$

$$\text{(R7)} \qquad OH + NO_2 \rightarrow HNO_3$$

Formation of peroxyacetylnitrate (PAN) is also a significant sink for odd hydrogen in some urban environments.

The division into NO_x-sensitive and ROG-sensitive photochemical regimes is determined by the relative size of (R5)-(R7) and their role as odd hydrogen sinks. When formation of nitric acid (R7) represents the major sink for odd hydrogen, then the equation of odd hydrogen sources and sinks demonstrates that OH must decrease with increasing NO_x. OH will also increase slightly with increasing ROG, reflecting the role of the latter as sources of odd hydrogen. The rate of ozone-producing reactions, being proportional to (R1), increases rapidly with increasing ROG and decreases with increasing NO_x. Alternatively, when formation of peroxides (reactions (R5) and (R6)) represents the major sink for odd hydrogen, then the concentration of HO_2 radicals is fixed by the size of the odd hydrogen source and is independent of NO_x. Because the odd hydrogen loss rate is proportional to $(HO_2)^2$, the HO_2 concentration also shows little sensitivity to ROG even when hydrocarbons form a significant source of odd hydrogen. The concentration of OH is governed by the interconversion of OH, HO_2, and RO_2 (reactions (R1)-(R4)). OH increases with increasing NO_x (due to (R3)) and decreases with increasing ROG (due to (R1)). The rate of ozone production increases with increasing NO_x but is insensitive to ROG, as increases in ROG coincide with decreases in OH.

Sillman et al. [1990b] have shown that reactions (R1)-(R7) lead to the following equation for OH, assuming that OH, HO_2, and RO_2 are in photochemical steady state with one another

based on reactions (R1)-(R4) and odd hydrogen sources and sinks are in similar steady state:

$$S_H = k_7[NO_2][OH] + \{k_5(\frac{k_4[CO]+k_1[RH]}{k_3[NO]})^2 + k_6\frac{k_4[CO]+k_1[RH]}{k_3[NO]}\frac{k_1[RH]}{k_2[NO]}\}[OH]^2 \quad (1)$$

where S_H represents the source of odd hydrogen from photolysis of ozone and aldehydes. The description of ROG-sensitive and NO_x-sensitive regimes follows directly from this equation, assuming that production of ozone is proportional to the rate of reaction (R1).

A link between ozone-NO_x-ROG sensitivity and the ratio H_2O_2/HNO_3 can be deduced from this simplified chemistry because both NO_x- versus ROG-sensitive ozone and the H_2O_2/HNO_3 ratio are dependent on the relative magnitude of (R5) and (R7). A similar link can be deduced for the ratio of organic peroxides (ROOH) to HNO_3, associated with the relative magnitude of (R6) and (R7). The well-known dependence of ozone-NO_x-ROG sensitivity on the ROG/NO_x ratio can also be deduced from this representation. A complete derivation is shown in the appendix.

Kleinman [1991, 1994] has described a similar transition between "NO_x-limited" and "radical-limited" photochemical regimes associated with season (summer versus winter) and demonstrated its link with peroxide concentrations. Their results suggest that moderately polluted environments in the eastern United States have NO_x-limited chemistry in summer and radical-limited chemistry in winter, associated with high and low peroxide concentrations, respectively. The NO_x-limited and radical-limited regimes of *Kleinman* [1991] are defined by the relative size of the source of odd hydrogen (S_H) relative to the NO_x source (S_N). The radical-limited regime is associated with conditions during nighttime and winter when OH-driven photochemistry virtually ceases due to lack of sunlight and H_2O. This is fundamentally different from ROG-sensitive urban photochemistry, which includes high OH and significant photochemical production of O_3, but there are direct parallels between the two. The relation between Kleinman's radical-limited regime and the urban ROG-sensitive regime is discussed further in the appendix.

Simulation Methods and Scenarios

Modeling results are based on simulated air pollution events in the northeast corridor (June 15, 1988) and Lake Michigan regions (August 2, 1988) [*Sillman et al.*, 1993]. Both these events featured O_3 in excess of 150 ppb and meteorology characterized by high temperatures (303°-306°K daytime) and water vapor (mixing ratio of 0.016), light winds, and restricted vertical mixing. Simulation methods are described in detail elsewhere [*Sillman et al.*, 1993]; a summary is given here. The simulations use the chemistry of *Lurmann et al.* [1986] with updated reaction rates [*DeMore et al.*, 1992], added $RO_2 + HO_2$ reactions [*Jacob and Wofsy*, 1988] and chemistry of isoprene and related species based on the work of *Paulson and Seinfeld* [1992]. Photolysis rates are based on those of *Madronich* [1987]. An aerosol optical depth of 0.68 was assumed, representing moderately polluted conditions typical of the eastern United States [*Flowers et al.*, 1969]. Other assumptions in the photolysis rate calculation included clear skies, a total O_3 column of 325 Dobson units (DU), surface albedo of 0.15, and single-scattering albedo of 0.75. Anthropogenic emissions are based on the National Acid Precipitation Assessment Program (NAPAP) 1980 [Environmental Protection Agency (EPA), 1986], and biogenic emissions are derived from data by *Lamb et al.* [1985] with land use data by *Matthews* [1983]. Deposition velocities over land were as follows: O_3 and NO_2, 0.6 cm s^{-1}; NO, 0.1 cm s^{-1}; HNO_3, cm s^{-1}; PAN, 0.25 cm s^{-1}; and H_2O_2, 1.0 cm s^{-1}. Deposition velocities over water were 0.05 cm s^{-1} for all these species.

The model includes urban subsections with 20 x 20 km horizontal resolution over domains of approximately 300 x 400 km in combination with simulated regional-scale photochemistry on a spatial domain that includes most of the eastern United States [Sillman et al., 1990a]. A vertical grid structure with variable heights is used to approximate the effect of the ocean and Lake Michigan in suppressing vertical mixing. Results represent average concentrations for the mixed layer. The mixing height during the daytime was derived from vertical temperature profiles and represents regionwide averages, but the model vertical structure includes low (200 m) mixing heights over water with an adjustment to represent the extent of vertical dispersion of land-based emissions transported over water.

Results for each scenario are derived from a simulated base case and subsequent simulations with emission rates for either anthropogenic ROG or NO_x reduced by 35% relative to emissions in the base case. In addition, a number of altered scenarios have been explored. These include (1) anthropogenic ROG emissions doubled from the inventory values (Lake Michigan), (2) anthropogenic ROG emissions cut in half from the inventory values (Lake Michigan), (3) zero biogenic emissions (northeast corridor), (4) height of the daytime mixed layer cut in half (northeast corridor), (5) biogenic emissions doubled from inventory values and height of the daytime mixed layer cut in half (northeast corridor).

The altered scenarios were designed to test the robustness of the indicator correlations and do not necessarily represent real events. However, it has been reported that emission rates for both anthropogenic and biogenic ROG may be twice as large as those reported in current inventories in the United States [*Fujita et al.*, 1992; *Geron et al.*, 1994]. Scenarios with ROG emissions lower than inventory values or with zero isoprene are unlikely to represent real conditions in the northeast corridor or Lake Michigan, but they may correspond to conditions in other environments (e.g., Europe or the southwestern United States).

NO_x-ROG Sensitivity and Indicator Species

The overall correlation between simulated O_3-NO_x-ROG sensitivity and potential indicator species will be illustrated for NO_y, which was discussed extensively by *Milford et al.* [1994]. Figure 1a shows the correlation between simulated sensitivity and NO_y for the Lake Michigan base case scenario. The figure shows several features that identify a good indicator species. There is a sharp delineation between NO_x-sensitive locations (corresponding to NO_y from 3 to 12 ppb), and ROG-sensitive locations (corresponding to NO_y from 11 to 50 ppb). The overlap between NO_x-sensitive locations and ROG-sensitive locations occupies a very narrow range of NO_y values (11-12 ppb) and the number of locations with NO_y in this range is a small fraction of the total model domain. In addition, the simulated NO_y extend over a wide range and are not clustered near the transition between NO_x- and ROG-sensitive locations.

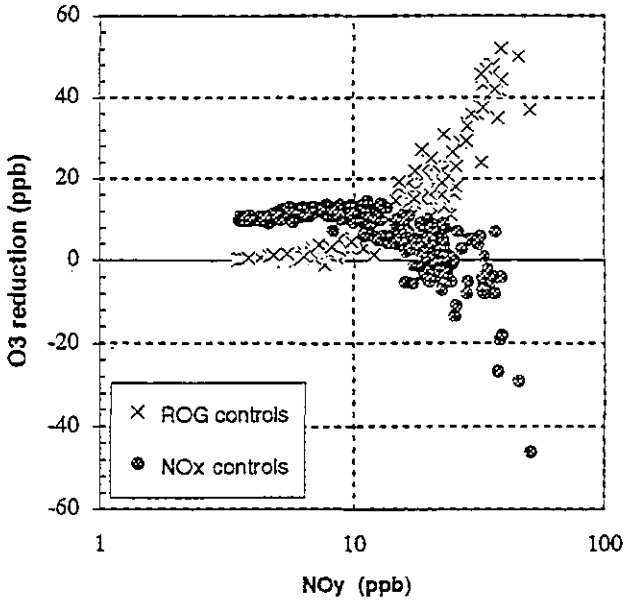

Figure 1a. Predicted reduction in peak O_3 (in parts per billion, or ppb) resulting from a 35% reduction in the emission rate for anthropogenic ROG (crosses) and from a 35% reduction in the emission rate for NO_x (circles), plotted against NO_y (ppb) coincident with the ozone peak in the simulation for the Lake Michigan base case scenario [from *Milford et al.*, 1994; *Sillman et al.*, 1993].

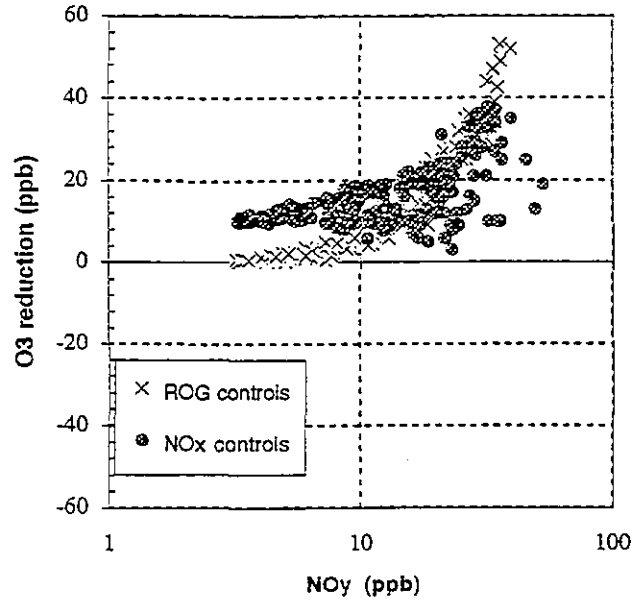

Figure 1b. Predicted reduction in peak O_3 (ppb) resulting from a 35% reduction in the emission rate for anthropogenic ROG (crosses) and from a 35% reduction in the emission rate for NO_x (circles), plotted against NO_y (ppb) coincident with the ozone peak in the simulation for the Lake Michigan scenario with doubled anthropogenic ROG [from *Milford et al.*, 1994].

When indicator values are located close to the NO_x-ROG transition point, the indicator-sensitivity correlation is likely to fall within the range of uncertainty associated with the model [e.g., *Milford et al.*, 1993].

Results from the Lake Michigan scenario with doubled ROG emissions (Figure 1b) illustrate a less successful correlation between sensitivity and NO_y. Here the range of NO_y values associated with both NO_x- and ROG-sensitive locations is much wider (16-32 ppb), and the number of locations with NO_y within this overlap region represents a significant fraction (43%) of the entire domain. A comparison with Figure 1a also shows that the range of NO_y associated with NO_x-sensitive O_3 has expanded and the range associated with ROG-sensitive NO_y has contracted in relation to the former scenario. Therefore NO_y as an indicator apparently fails to account for the change in sensitivity that would result from a doubling of base case anthropogenic ROG.

The good correlation between sensitivity and NO_y in Figure 1a and the comparatively poor correlation in Figure 1b can be summarized by recording the following parameters for each model scenario: scenario (a), the range of indicator values associated with NO_x-sensitive locations (defined as locations where the simulated reduction in peak O_3 associated with reduced NO_x exceeds the simulated reduction associated with reduced ROG by > 5 ppb); scenario (b), the range of indicator values associated with ROG-sensitive locations (defined similarly); and scenario (c), the "20% uncertainty fraction," equal to the fraction of the model domain with indicator values that are within 20% of the range of indicator values associated with the opposite NO_x-ROG sensitivity. These parameters are recorded for each indicator and each scenario in Table 1 and will be the basis for identifying their usefulness. Results for each indicator will be discussed here.

NO_y. The use of NO_y as an indicator for sensitivity was discussed in detail by *Milford et al.* [1994] and has been illustrated in Figure 1. The two cases in Figure 1 illustrate both the positive and negative features of NO_y as an indicator.

As shown in Table 1, most of the individual simulations show a strong correlation between sensitivity and NO_y with a broad range of simulated NO_y concentrations and a relatively narrow range overlap between NO_x- and ROG-sensitive locations. Results from *Milford et al.* [1994] showed a similar strong correlation and similar ranges of transition between NO_x- and ROG-sensitive NO_y. However, the transition point between NO_x- and ROG-sensitive locations tends to shift in response to changes in anthropogenic and biogenic ROG. Referring to Table 1, the transition occurs at ~10 ppb in simulations with little or no biogenic ROG (Lake Michigan base scenario and northeast corridor scenario with zero isoprene). The northeast corridor base scenario has significantly more biogenic ROG than Lake Michigan and a higher transition (~20 ppb), and the northeast corridor scenario with doubled isoprene has a transition at ~35 ppb. Similarly, the Lake Michigan scenario with doubled anthropogenic ROG (Figure 1b) has a higher transition than the base scenario. By contrast the northeast scenario with a low mixed layer has a transition point (22 ppb) virtually identical with the base scenario.

The rationale for NO_y as an indicator is based in part on the impact of stagnant meteorology on NO_x-ROG sensitivity. Stagnant meteorology and associated high NO_x, ROG, and NO_y cause an increase in the photochemical lifetimes of NO_x and ROG, with the result that an aging urban plume remains in the ROG-sensitive regime for a longer period of time. With more vigorous meteorological dispersion and lower NO_x, ROG, and NO_y an aging urban plume would rapidly become NO_x sensitive [*Milford et al.*, 1994]. The contrast between the northeast

Table 1. NO_x and ROG-Sensitive Ranges for Indicator Species

Model Scenario	Indicator					
	NO_y, ppb	$NO_y - NO_x$, ppb	$\frac{O_3}{NO_y}$	$\frac{O_3}{NO_y - NO_x}$	$\frac{O_3 - 40\ ppb}{NO_y - NO_x}$	$\frac{O_3}{HNO_3}$
Lake Michigan Base Case Scenario						
(a) NO_x range	4-11	3-9	7.2-17	9.5-19	4.8-8.8	12-45
(b) ROG range	11-50	10-33	1.9-7.4	3.5-8.4	2.0-5.5	4.1-12
(c) Uncertainty	0.17	0.12	0.27	0.13	0.49	0.15
Lake Michigan Scenario with Doubled Anthropogenic ROG						
(a) NO_x range	4-31	3-29	6.9-17	7.3-19	5.2-9.1	10-52
(b) ROG range	16-52	13-45	3.8-7.8	4.8-8.7	3.4-6.4	6.7-15
(c) Uncertainty	0.54	0.53	0.57	0.54	0.75	0.54
Lake Michigan Scenario With Anthropogenic ROG Reduced by 50%						
(a) NO_x range	4-12	3-11	6.5-17	7.2-21	3.6-8.7	8.5-47
(b) ROG range	14-35	9-26	2.2-6.4	3.6-8.9	1.8-4.9	4.0-12
(c) Uncertainty	0.11	0.32	0.18	0.32	0.41	0.28
Lake Michigan Base Case Scenario, Sensitivity of O_3 at Noon						
(a) NO_x range	3-7	2-5	9.0-22	14-25	5.3-7.8	11-56
(b) ROG range	9-65	6-18	0.9-7.0	3.1-11	0.7-4.9	3.5-16
(c) Uncertainty	0.03	0.13	0.04	0.09	0.20	0.29
Northeast Corridor Base Case Scenario						
(a) NO_x range	4-22	4-19	5.6-19	7.9-21	5.3-11	14-86
(b) ROG range	16-34	11-23	3.4-7.1	6.2-8.6	4.1-5.6	9.6-16
(c) Uncertainty	0.14	0.29	0.10	0.15	0.11	0.15
Northeast Corridor Scenario With Zero Isoprene						
(a) NO_x range	3-8	3-6	10-19	14-22	6.4-11	17-34
(b) ROG range	10-30	7-21	3.0-11	5.7-13	1.5-7.4	7.3-20
(c) Uncertainty	0.09	0.09	0.33	0.26	0.91	0.75
Northeast Corridor With Mixed Layer Reduced by 50%						
(a) NO_x range	5-26	4-22	4.1-19	7.5-20	5.3-11	14-92
(b) ROG range	19-44	10-30	2.5-7.4	5.2-9.0	3.7-6.3	8.0-16
(c) Uncertainty	0.17	0.36	0.15	0.20	0.18	0.18
Northeast Corridor With Doubled Isoprene and Mixed Layer Reduced by 50%						
(a) NO_x range	5-38	5-31	3.0-19	6.1-19	4.5-11	11-180
(b) ROG range	34-44	19-31	3.0-5.2	6.3-7.0	4.8-5.3	11-15
(c) Uncertainty	0.02	0.15	0.04	0.07	0.12	0.04

corridor base scenario and the scenario with a low mixed layer demonstrates the impact of stagnant meteorology. The base scenario is dominated by NO_x-sensitive photochemistry, but the scenario with a low mixed layer has an extensive ROG-sensitive region. The difference in NO_x-ROG sensitivity between these two scenarios is reflected by higher NO_y in the latter, and the transition between NO_x- and ROG-sensitive photochemistry occurs at virtually the same NO_y in each (20-22 ppb). NO_y as an indicator can also be explained in terms of ROG/NO_x ratios if reactivity-weighted ROG remains relatively constant, as suggested by *Chameides et al.* [1992]. The changes in the transition point for NO_y in simulations with different ROG are consistent with the well-known dependence of NO_x-ROG sensitivity on ROG/NO_x ratios.

The transition point for NO_y also varies with the photochemical age of an air mass. Ozone formation is more likely to be sensitive to ROG in locations close to emission sources, and the associated transition between NO_x- and ROG-sensitive chemistry is likely to occur at lower NO_y. This effect can be illustrated by comparing ozone-NO_y-ROG sensitivity early in the day with sensitivity associated with peak O_3, usually in middle or late afternoon. As shown in Table 1, the sensitivity of O_3 at noon in the Lake Michigan base scenario correlates with NO_y, but the transition point is shifted toward lower NO_y (8 ppb versus 11 ppb for peak O_3).

The sum of NO_x reaction products (= NO_y - NO_x) can also be used as an indicator for sensitivity and is included in Table 1. $NO_y - NO_x$ has an advantage over NO_y as an indicator because

Table 1. (continued)

Model Scenario	Indicator				
	$\frac{HCHO}{NO_y}$	$\frac{HCHO-5\ ppb}{NO_y}$	$\frac{H_2O_2}{HNO_3}$	$\frac{H_2O_2}{NO_y - NO_x}$	$\frac{H_2O_2}{NO_y}$
Lake Michigan Base Case Scenario					
(a) NO_x range	0.29-0.67	0.79-1.9	0.37-2.3	0.27-0.97	0.22-0.82
(b) ROG range	0.14-0.31	0.28-0.73	0.01-0.30	0.01-0.25	0.007-0.24
(c) Uncertainty	0.30	0.16	0.03	0.11	0.16
Lake Michigan scenario with doubled anthropogenic ROG					
(a) NO_x range	0.35-0.76	0.55-2.0	0.25-2.8	0.17-1.0	0.16-0.89
(b) ROG range	0.23-0.42	0.42-067	0.03-0.36	0.02-0.23	0.02-0.22
(c) Uncertainty	0.64	0.55	0.34	0.38	0.40
Lake Michigan scenario with anthropogenic ROG reduced by 50%					
(a) NO_x range	0.20-0.66	0.60-1.9	0.26-2.4	0.21-1.1	0.18-0.84
(b) ROG range	0.10-.23	0.26-0.56	0.03-0.29	0.02-0.22	0.01-0.16
(c) Uncertainty	0.34	0.16	0.16	0.16	0.11
Lake Michigan Base Case Scenario, SNoon					
(a) NO_x range	0.39-0.82	1.1-2.8	0.67-2.2	0.31-1.1	0.27-1.0
(b) ROG range	0.11-0.36	0.22-0.82	0.008-0.38	0.01-0.28	0.002-0.15
(c) Uncertainty	0.17	0.04	0	0.06	0
Northeast Corridor Base Case Scenario					
(a) NO_x range	0.26-1.2	0.55-2.2	0.43-6.1	0.24-1.6	0.22-1.5
(b) ROG range	0.23-0.42	0.41-0.67	0.19-0.54	0.12-0.29	0.09-0.23
(c) Uncertainty	0.57	0.18	0.08	0.08	0.02
Northeast corridor scenario with zero isoprene					
(a) NO_x range	0.26-0.52	0.92-1.7	0.61-1.5	0.48-1.2	0.39-1.1
(b) ROG range	0.17-.38	0.37-0.83	0.10-0.64	0.08-0.50	0.05-0.45
(c) Uncertainty	0.93	0.17	0.16	0.15	0.21
Northeast Corridor With Mixed Layer Reduced by 50%					
(a) NO_x range	0.28-1.3	0.54-2.2	0.46-7.0	0.24-1.5	0.15-1.4
(b) ROG range	0.25-0.52	0.36-0.77	0.12-0.55	0.08-0.35	0.05-0.33
(c) Uncertainty	0.62	0.28	0.07	0.12	0.13
Northeast Corridor With Doubled Isoprene and Mixed Layer Reduced by 50%					
(a) NO_x range	0.33-1.8	0.49-2.6	0.45-20.	0.20-1.6	0.15-1.5
(b) ROG range	0.32-0.43	0.43-0.56	0.20-0.62	0.11-0.28	0.08-0.17
(c) Uncertainty	0.09	0.04	0.04	0.05	0.01

The range of indicator values associated with (a) NO_x-sensitive chemistry and (b) ROG-sensitive chemistry is given for each simulation, along with (c) the fraction of model indicator values associated with uncertain NO_x-ROG sensitivity. The NO_x-sensitive range is defined as the range of locations with simulated peak O_3 in simulations with reduced NO_x lower than in simulations with reduced ROG by at least 5 ppb. The ROG-sensitive range is defined analogously. The uncertainty fraction is defined by the fraction of the model domain with indicator values within 20% of the indicator range associated with the opposite NO_x-ROG sensitivity.

NO_y field measurements in urban locations may be impacted by on-site NO_x emission sources. However, the correlation between sensitivity and NO_y - NO_x in models is somewhat worse than the correlation with NO_y, with a broader overlap between NO_x-sensitive and ROG-sensitive ranges (Table 1). Transition points for NO_y - NO_x are ~30% lower than the corresponding transition point for NO_y in these simulations. The subsequent indicator ratios based on NO_y can all be used with NO_y - NO_x substituted for NO_y and with the same 30% change in transition values.

$\frac{O_3}{NO_y - NO_x}$ and $\frac{O_3 - 40ppb}{NO_y - NO_x}$. The slope of O_3 versus NO_y or O_3 versus NO_x reaction products (NO_y - NO_x) has been used

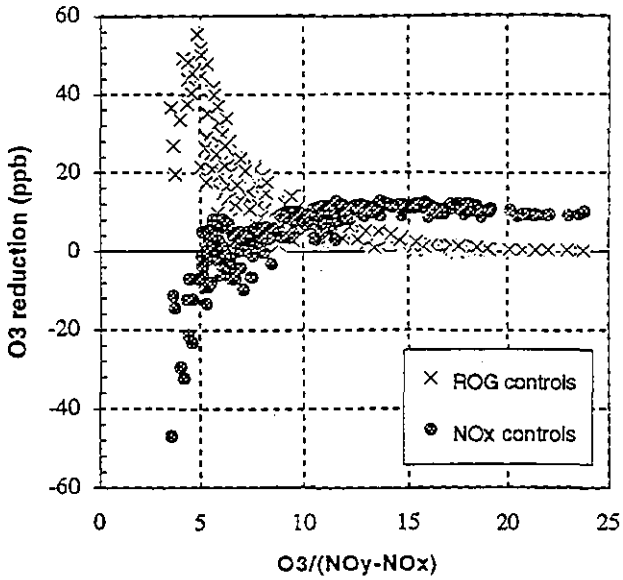

Figure 2a. Predicted reduction in peak O_3 (ppb) resulting from a 35% reduction in the emission rate for anthropogenic ROG (crosses) and from a 35% reduction in the emission rate for NO_x (circles), plotted against $O_3/(NO_y - NO_x)$ coincident with the ozone peak in the simulation for the Lake Michigan base case scenario.

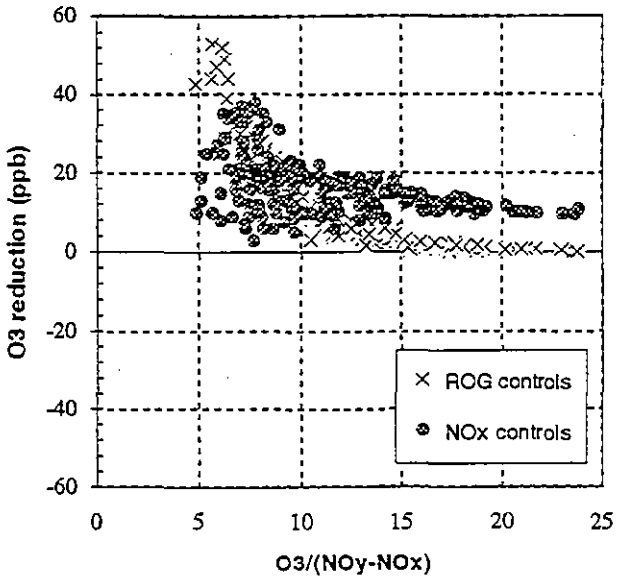

Figure 2b. Predicted reduction in peak O_3 (ppb) resulting from a 35% reduction in the emission rate for anthropogenic ROG (crosses) and from a 35% reduction in the emission rate for NO_x (circles), plotted against $O_3/(NO_y - NO_x)$ coincident with the ozone peak in the simulation for the Lake Michigan scenario with doubled anthropogenic ROG.

frequently to analyze photochemistry of O_3 in polluted rural areas [*Sillman et al.*, 1990b; *McKeen et al.*, 1991; *Trainer et al.*, 1993]. The ratio $(O_3 - 40\ ppb)/(NO_y - NO_x)$ can be used from individual measurements to quantify the slope, where 40 ppb represents background O_3 both in the current simulations and in the measured correlations between O_3 and $NO_y - NO_x$ of *Trainer et al.* [1993].

A rationale for either O_3/NO_y or $(O_3 - 40\ ppb)/NO_y$ as indicator for NO_x-ROG sensitivity can be derived from the analysis of odd hydrogen in the appendix. The transition from NO_x- to ROG-sensitive chemistry is associated with the ratio of sources of odd hydrogen (S_H) to a modified sum of NO_x reaction products ($NO_y - NO_x + HNO_3$) (equation (A6)). If the source of odd hydrogen is proportional to $[O_3]$, then the transition criterion given by (A6) is approximately correlated to the ratio $O_3/(NO_y - NO_x)$. Alternatively, if the source of odd hydrogen is proportional to the rate of production of ozone, then the transition criterion is equivalent to a constant slope of O_3 versus $NO_y - NO_x$. The slope of O_3 versus $NO_y - NO_x$ has also been discussed in terms of production efficiencies for O_3 [*Liu et al.*, 1987; *Lin et al.*, 1988].

Results for both indicators are shown in Figure 2 and Table 1. The performance of $O_3/(NO_y - NO_x)$ as an indicator is comparable to NO_y with a well-defined transition between NO_x-sensitive chemistry ($O_3/(NO_y - NO_x) > 9$) and ROG-sensitive chemistry ($O_3/(NO_y - NO_x) < 8$). In contrast to NO_y, the transition point for $O_3/(NO_y - NO_x)$ shows relatively little variation among the model scenarios. For example, the transition points for $O_3/(NO_y - NO_x)$ in the Lake Michigan base- and doubled-ROG scenarios (Figures 2a and 2b) are virtually identical. By contrast, the transition point for NO_y changed by a factor of 2 between the scenarios. Significant differences in the transition point for $O_3/(NO_y - NO_x)$ only appear for the northeast corridor scenarios with zero isoprene (transition at $O_3/(NO_y - NO_x) \cong 13$) and doubled isoprene (transition at $O_3/(NO_y - NO_x) \cong 6$). The correlation with sensitivity at noon also shows a different transition point ($O_3/(NO_y - NO_x) \cong 13$). The ratio O_3/NO_y also performs well as an indicator in these simulations (transition point at O_3/NO_y = 6-7), although $O_3/(NO_y - NO_x)$ is correct in terms of theory. The ratio O_3/HNO_3 also performs well.

The ratio $(O_3 - 40\ ppb)/(NO_y - NO_x)$ (Figure 3 and Table 1) is less successful as in indicator than $O_3/(NO_y - NO_x)$. Although

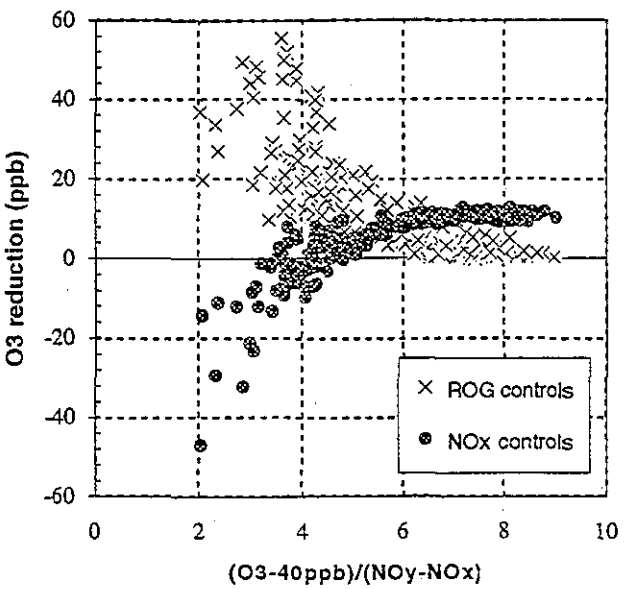

Figure 3. Predicted reduction in peak O_3 (ppb) resulting from a 35% reduction in the emission rate for anthropogenic ROG (crosses) and from a 35% reduction in the emission rate for NO_x (circles), plotted against $(O_3 - 40\ ppb)/(NO_y - NO_x)$ coincident with the ozone peak in the simulation for the Lake Michigan base case scenario.

the transition point associated with $(O_3 - 40\ ppb)/(NO_y - NO_x)$ is generally consistent among the seven model scenarios, a large proportion of indicator values are located very close to the transition region. Consequently, the fraction of the model domain associated with or close to the region of overlap between NO_x- and ROG-sensitive ranges is larger than that for NO_y or $O_3/(NO_y - NO_x)$. The ratio $(O_3 - 40\ ppb)/NO_y$ performs similarly. The ratio $(O_3 - 40\ ppb)/NO_y$ is especially interesting because it is directly comparable to the AIRTRAK method [*Johnson*, 1984; *Johnson et al.*, 1990; *Blanchard et al.*, 1993], which is being investigated for regulatory use by the U.S. Environmental Protection Agency as a basis for identifying NO_x- versus ROG-sensitive chemistry. *Johnson et al.* derived an indicator for NO_x-ROG sensitivity equivalent to $(O_3 - 40\ ppb)/NO_y$, using results from smog chambers, and identified the transition point as $(O_3 - 40\ ppb)/NO_y = 4.09$. The simulations here have a transition point at $(O_3 - 40\ ppb)/NO_y = 3$–4 but with considerable scatter.

Both $O_3/(NO_y - NO_x)$ and $(O_3 - 40\ ppb)/(NO_y - NO_x)$ are associated in theory with rates of production for odd hydrogen. Consequently, it is likely that transition points will shift in simulations with different amounts of solar radiation of H_2O, both of which affect the odd hydrogen source term, and with temperature, which affects PAN.

HCHO/NO_y. Figure 4 shows the correlation between NO_x-ROG sensitivity and the ratio $HCHO/NO_y$ at the time of the ozone peak. The ratio $HCHO/NO_y$ functions as a reactivity-weighted ROG/NO_x ratio, since production of HCHO is roughly proportional to the summed rate of reactions of ROG with OH. Low $HCHO/NO_y$ is associated with ROG-sensitive ozone, a result that parallels the relation between ozone sensitivity and ROG/NO_x. Other ROG-based indicators, including reactivity-weighted total ROG and ROG/NO_x and ROG/NO_y ratios, did not provide a good correlation with ozone-NO_x-ROG sensitivity in the simulations. The ratio $HCHO/(NO_y - NO_x)$ can also be associated with NO_x-ROG sensitivity through the analysis of odd hydrogen, as was done for $O_3/(NO_y - NO_x)$, with the assumption that the odd hydrogen source is proportional to HCHO.

The correlation between sensitivity and $HCHO/NO_y$ is comparable with NO_y in its consistency, although its usefulness is partially compromised by its relatively narrow range of values. The model predicts the crossover between NO_x-sensitive and ROG-sensitive ozone occurs at $HCHO/NO_y \cong 0.28$, while the ROG-sensitive Chicago urban plume is predicted to have $HCHO/NO_y \cong 0.20$. In highly polluted ROG-sensitive environments the ratio appears to approach 0.15 as an asymptotic limit. The clustering of $HCHO/NO_y$ close to the transition point is reflected in the large fractions of the model domain associated with overlap between NO_x- and ROG-sensitive ranges (Table 1).

An interesting feature of $HCHO/NO_y$ as an indicator is that the $HCHO/NO_y$ correlations represent the impact of changes in ROG emissions. $HCHO/NO_y$ can be combined with NO_y to form an indicator $((HCHO + 5\ ppb)/NO_y)$ with a transition point that shows relatively small variations in response to changed model emission rates for ROG (see Table 1).

H_2O_2/HNO_3. The connection between NO_x-ROG sensitivity and the ratio of hydrogen peroxide to nitric acid is stronger than for the other indicators in terms of both theory and simulation results. It was shown in section 2 and the appendix (Equation (A6)) that NO_x-ROG sensitivity is linked to the relative rates of formation of peroxides and nitric acid and to their role as sinks for odd hydrogen. Simulation results (Figure 5 and Table 1) show a close correlation between H_2O_2/HNO_3 and sensitivity for all model scenarios. The overlap between NO_x- and ROG-sensitive ranges is consistently small in comparison with the range of simulated values for H_2O_2/HNO_3,

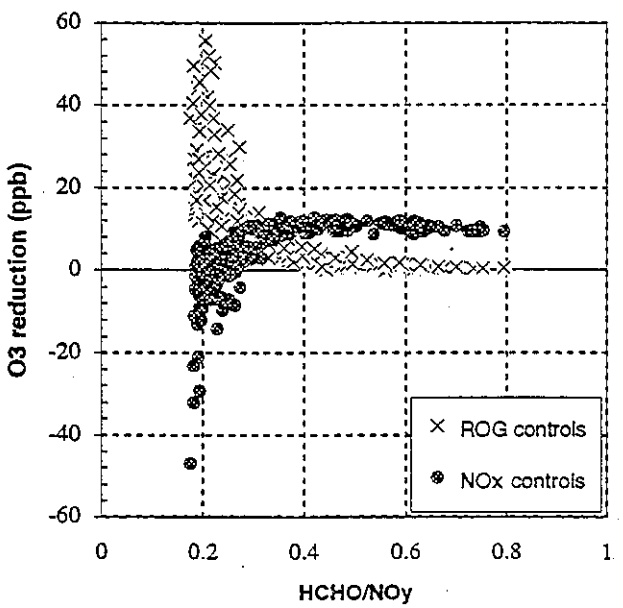

Figure 4. Predicted reduction in peak O_3 (ppb) resulting from a 35% reduction in the emission rate for anthropogenic ROG (crosses) and from a 35% reduction in the emission rate for NO_x (solid circles), plotted against $HCHO/NO_y$ coincident with the ozone peak in the simulation for the Lake Michigan base case scenario.

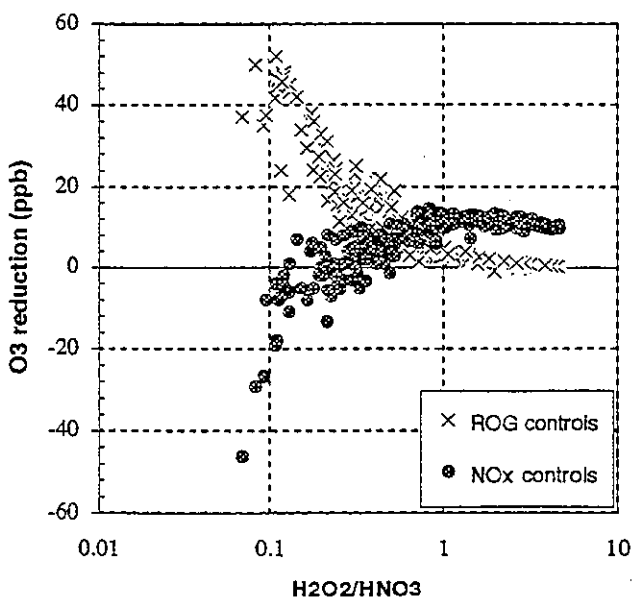

Figure 5. Predicted reduction in peak O_3 (ppb) resulting from a 35% reduction in the emission rate for anthropogenic ROG (crosses) and from a 35% reduction in the emission rate for NO_x (solid circles), plotted against H_2O_2/HNO_3 coincident with the ozone peak in the simulation for the Lake Michigan base case scenario.

and the "uncertainty fractions" are low in comparison with the other indicators. The transition from NO_x- to ROG-sensitive chemistry occurs at $H_2O_2/HNO_3 \cong 0.3$-0.5 and shows relatively small variation among the model scenarios. The northeast corridor scenario with zero isoprene has a signficantly higher transition ratio (0.6), and the northeast scenarios all have slightly higher transition points than the Lake Michigan scenarios. In contrast to the previous indicators, the sensitivity correlation for H_2O_2/HNO_3 for O_3 at noon shows the same transition point as the correlations for peak O_3. Table 1 also shows indicator correlations for H_2O_2/NO_y, which might be used in place of H_2O_2/HNO_3 if HNO_3 measurements are unavailable.

Uncertainties. The extent of overlap between NO_x-sensitive and ROG-sensitive ranges for indicator species and the comparison between indicator transition points in different model scenarios provides a partial representation of the uncertainties associated with the sensitivity-indicator correlations. The use of model-based correlations also involves additional uncertainties based on model assumptions or omissions. Some of these uncertainties will be discussed here.

All of the indicators include at least one species (HNO_3) which has a high rate of surface deposition. Another species (H_2O_2) may form an aerosol in the presense of haze (C. Walcek, State University of New York at Albany, private communication, 1994). The indicator values reported here are therefore sensitive to assumed deposition and aerosol formation rates. The impact of deposition in the models can be seen by comparing transition points for the northeast corridor scenario with zero isoprene with transition points for other scenarios. The zero-isoprene scenario is unusual in that ROG-sensitive chemistry persists in urban plumes for a period of more than 24 hours downwind from emission sources, allowing for much greater deposition of HNO_3 during transport associated with the transition region. Day-old urban plumes all have NO_x-sensitive chemistry in the other scenarios. Table 1 shows that transition points in the zero-isoprene scenario are different from the other scenarios for every indicator, and that the difference is consistent with a higher rate of removal for HNO_3 at the transition point. Differences in model deposition rates also affect predicted cross-species correlations (below).

The impact of solar radiation, $[H_2O]$ or temperature on indicator correlations has not been explored. At least one indicator ($O_3/(NO_y - NO_x)$) is expected to vary significantly in response to changes in radiation and $[H_2O]$, which affect production rates for odd hydrogen. Temperature affects formation rates for PAN and therefore may also have an impact on the performance of indicators involving NO_y.

All model calculations are sensitive to uncertainties in chemical rate constants and stoichiometry, which generally cause a 20-30% uncertainty in resulting species concentrations [*Milford et al.*, 1993]. H_2O_2 is especially vulnerable to reaction rate and mechanism uncertainties. H_2O_2 is closely associated with model formation of organic peroxides RO_2 + HO_2 reactions (R6), which varies significantly among different photochemical mechanisms. In the current simulation the formation of organic peroxides via (R6) is approximately half the rate of formation of H_2O_2, but this simulated rate has not been compared with atmospheric measurements. Formation of H_2O_2 and some organic peroxides (e.g., $HOCH_2OOH$) from reactions other than (R6) has not been included and adds further uncertainty to the interpretation of H_2O_2 and organic peroxide concentrations.

Correlations Between Indicator Species

The proposed connection between NO_x-ROG sensitivity and indicator species would be strengthened if the simulations could also be used to generate correlations between indicator species that could be tested against measurements. Unfortunately, the simulations predict no strong correlations among all the indicator species apart from the O_3 - NO_y correlation explored by *Trainer et al.* [1993].

Figures 6 and 7 show simulated correlations between the species associated with indicator ratios, HCHO versus NO_y and H_2O_2 versus HNO_3. Results illustrate the differences between the largely NO_x-sensitive chemistry in the northeast corridor base case scenario and the largely ROG-sensitive chemistry in

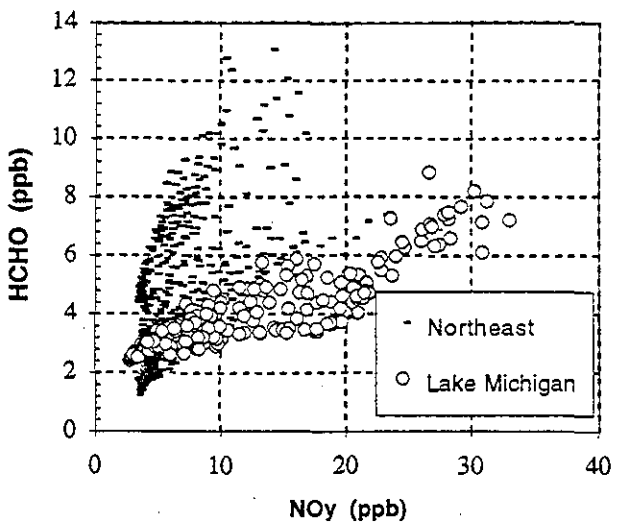

Figure 6. HCHO versus NO_y (ppb) at 1800 LT in simulations for the northeast corridor (points) and the Lake Michigan airshed (circles).

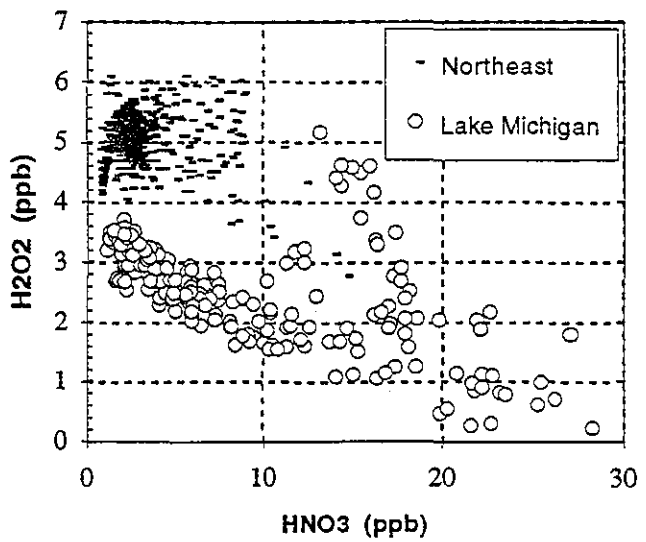

Figure 7. H_2O_2 versus HNO_3 (ppb) at 1800 LT in simulations for the northeast corridor (points) and the Lake Michigan airshed (circles).

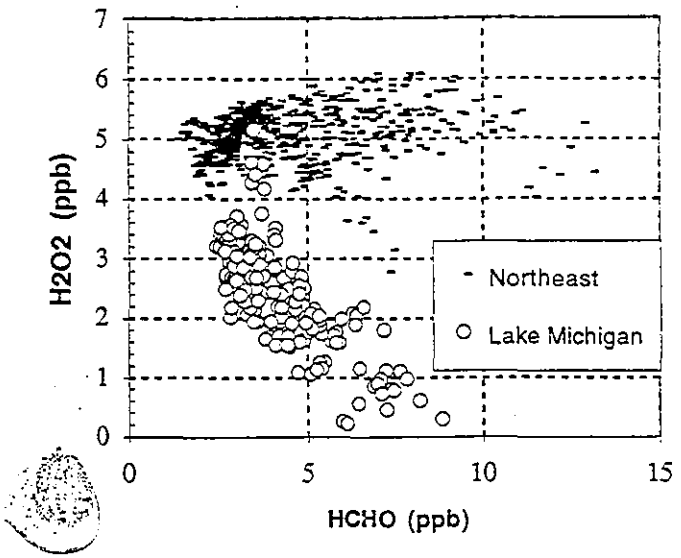

Figure 8. H_2O_2 versus HCHO (ppb) at 1800 LT in simulations for the northeast corridor (points) and the Lake Michigan airshed (circles).

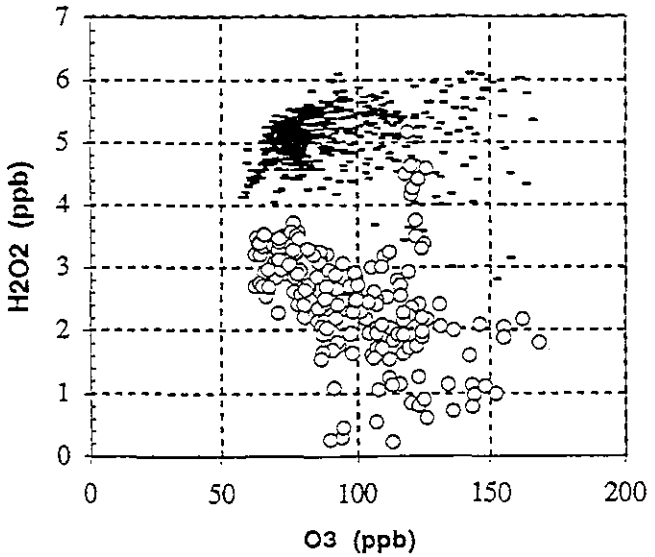

Figure 9. H_2O_2 versus O_3 (ppb) at 1800 LT in simulations for the northeast corridor (points) and the Lake Michigan airshed (circles).

the Lake Michigan base case. HCHO increases versus NO_y with two distinct slopes, apparently corresponding to NO_x- versus ROG-sensitive chemistry. The distinct slopes may also represent the difference between photochemical evolution of combined anthropogenic and biogenic emissions over land versus evolution of urban plumes transported over water with little biogenic emission. H_2O_2 and HNO_3 anticorrelate with each other, but the northeast corridor simulation has higher H_2O_2 and a weaker anticorrelation than the Lake Michigan simulation. The lack of a consistent correlation among these species is partially explained by their tendency to assume different correlative patterns in NO_x- versus ROG-sensitive conditions.

There is also no consistent correlation between the simulated H_2O_2 and HCHO or between H_2O_2 and O_3 (Figures 8 and 9). However, there is an intriguing triple correlation among O_3, H_2O_2, and NO_x reaction products. In theory (see appendix) the sum $H_2O_2 + NO_y - NO_x$ represents the cumulative sink for odd hydrogen and may be expected to correlate with O_3. A correlation of this type is predicted in the simulation for the northeast corridor (Figure 10a), where O_3 versus $H_2O_2 + NO_y - NO_x$ shows a stronger correlation that O_3 versus $NO_y - NO_x$ or O_3 versus HNO_3. A weaker pattern appears in the Lake Michigan simulation (Figure 10b), although the correlation between O_3 and $H_2O_2 + NO_y - NO_x$ is again stronger than the correlation between O_3 and reactive nitrogen. A significant part of the poor correlation in Figure 9b is due to the change in surface deposition rates between the land and the lake shore in the model. The high $H_2O_2 + NO_y - NO_x$ versus O_3 all corresponds to locations associated with transport over Lake Michigan, where model deposition rates are low. The low ratios in Figure 10b represent locations over land and are similar to the ratios in the northeast corridor simulation (Figure 10a).

Although difficult to measure, the predicted $H_2O_2 + NO_y - NO_x$ versus O_3 and its interpretation in terms of odd hydrogen may represent an extension of the rural O_3 versus $NO_y - NO_x$ to urban environments. The viewpoint here is different from that of *Liu et al.* [1987], *Lin et al.* [1988], *McKeen et al.* [1991], and *Trainer et al.* [1993], who emphasize the role of NO_x as precursor for O_3 and the slope O_3 versus $NO_y - NO_x$ as a representation of varying production efficiencies for O_3. The view presented here emphasizes O_3 as a source for odd hydrogen, either directly or through association with intermediate hydrocarbons, and rates of formation for both peroxides and reactive nitrogen as limited by the size of the odd hydrogen source. The transition from NO_x- to ROG-sensitive chemistry is linked with the replacement of peroxides by HNO_3 as the dominant sink for odd hydrogen, and therefore by a decreasing ratio of O_3 to reactive nitrogen.

Comparison With Observations

In recent years, concurrent measurements of NO_y, HCHO, H_2O_2, and HNO_3 have been made in Claremont, California, near Los Angeles (Bart Croes, State of California Air Resources Board, Sacramento, California, private communication, 1994), in Atlanta, Georga [*Sillman et al.*, 1995], and at a rural site in Virginia [*Jacob et al.*, 1995]. Complete analyses of field measurements will be provided in papers authored by the principal investigators, but results have been graciously provided. Because some results are preliminary, they have large uncertainties (+/- 25%) but they provide evidence for cross correlation among the indicator species.

As shown in Table 2, measured values during an event at Claremont, California are consistent with ROG-sensitive chemistry. These included very high (> 50 ppb) afternoon NO_y, low (< 1 ppb) H_2O_2, and an HCHO/NO_y ratio of 0.16. The ROG-sensitive nature of ozone in Claremont is consistent with published modelling studies for the region [*Milford et al.*, 1989], although model results also suggest that the chemistry becomes sensitive to NO_x at downwind locations within greater Los Angeles.

Measured concentrations for Atlanta are more difficult to interpret because NO_y was only availale from helicopter-based measurements 40 km downwind from Atlanta, while H_2O_2 and HCHO were measured at a site near downtown. Helicopter-based

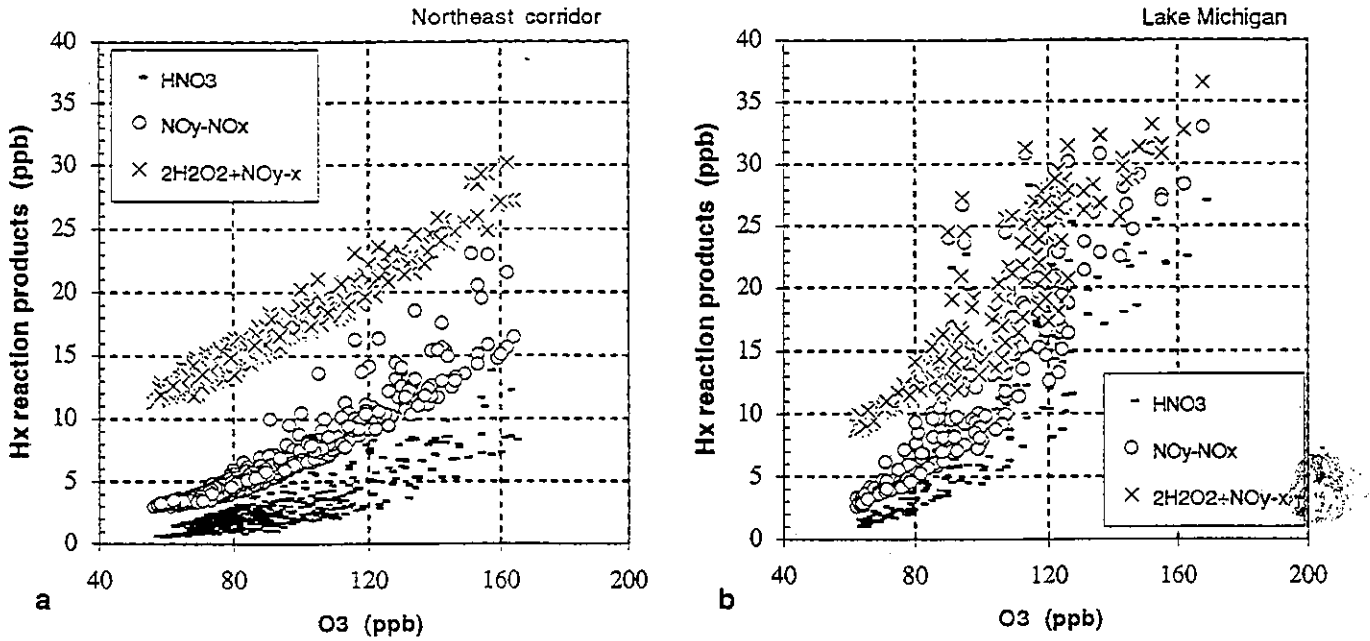

Figure 10. HNO_3 (points) , NO_y - NO_x (circles) and H_2O_2 + (NOy - NOx) (crosses) versus O_3, all in ppb at 1800 LT in simulations for (a) the northeast corridor and (b) the Lake Michigan airshed.

measurements at 600 m found ~12 ppb NO_y coincident with peak O_3 (143 ppb), values which are consistent with models [*Sillman et al.*, 1995]. Given the high emission rate for isoprene in Atlanta, the measured NO_y and O_3/NO_y both suggest NO_x-sensitive ozone. However, surface measurements of HCHO at South Dekalb, ~5 km from the helicopter measurements, were lower than would be expected in a NO_x-sensitive environment and lower than those predicted by photochemical models [*Sillman et al.*, 1995. Peroxides (3.5 ppb) were measured near downtown, but up to 50% of this total may represent organic peroxides other than H_2O_2 [*Sillman et al.*, 1995; *Lee et al.*, 1993]. The resulting values for both $HCHO/NO_y$ and H_2O_2/NO_y (see Table 2) suggest NO_x-sensitive chemistry but lie close to the transition point. All four indicators show a large contrast between Claremont and Atlanta, suggesting that chemistry is fundamentally different in the two locations.

Jacob et al. [1995] measured NO_y and H_2O_2 at a site in rural Virginia during September and October 1990. They reported a significant variation in H_2O_2/NO_y ratios between the beginning and the end of the time period, which corresponded to a sharp decrease in solar radiation, H_2O, and biogenic emission of isoprene at the start of autumn. The measured H_2O_2/NO_y ratio on a day with high O_3 in early September, shown in Table 2, was higher than that in the Atlanta measurements and is consistent with predictions of NO_x-sensitive O_3 in rural eastern North America [*Sillman et al.*, 1990b; *McKeen et al.*, 1991; *Possiel et al.*, 1991]. As discussed by *Jacob et al.* [1995], the sharp drop in H_2O_2/NO_y between September and October may be associated with a shift

Table 2. Measured Concentrations of Indicator Species

Species	Claremont, California,[a] June 25, 1987, 1300 LT	Atlanta, Georgia,[b] August 10, 1990, 1700 LT	Virginia,[c] September 12, 1990, 1500 LT
O_3	200	(143)	75
NO_y	65	(12)	4
HCHO	10.5	4	...
H_2O_2	0.99	(3.5)	1.5
HNO_3	20	...	
O_3/NO_y	3.1	(12)	19
$HCHO/NO_y$	0.16	(0.33)	...
H_2O_2/NO_y	0.017	(0.1-5-0.3)	0.38
H_2O_2/HNO_3	0.05		

a From B. Croes (private communication, 1994).

b Ratios for Atlanta are based on helicopter observations of the plume 30 km southeast of Atlanta, coincident with peak O_3 at 600 m. HCHO and H_2O_2 were observed at the Georgia Tech campus near downtown. From *Sillman et al.* [1995].

c From Jacob et al. [1995].

toward ROG-sensitive chemistry during the winter. *Kleinman* [1991] also discusses the seasonal shift from NO_x-sensitive to ROG-sensitive chemistry in eastern North America and correlates it with changes in measured H_2O_2.

Conclusions

Model predictions for O_3-NO_x-ROG sensitivity have been shown to correlate with simulated values for four indicator species: NO_y, $O_3/(NO_y - NO_x)$, (HCHO-5 ppb)/$(NO_y - NO_x)$, and H_2O_2/HNO_3, all coincident with the ozone peak. The derived correlations between ozone sensitivity and the indicator species change somewhat when model assumptions are altered, but the model correlations remain at least partially valid, even when model emission rates are stretched far beyond the range of currently accepted values. The sensitivity correlations for $O_3/(NO_y - NO_x)$ and H_2O_2/HNO_3 appear to be robust and are not affected by changes in model assumptions, although they may be affected by changes (e.g., solar radiation, and aerosol formation) not included here. The connection between these species and NO_x-ROG sensitivity has also been explained in terms of the fundamental chemistry of O_3, NO_x, and ROG.

The correlations suggest that the indicator species may provide a powerful tool in assessing the relative effectiveness of ROG versus NO_x controls and also will provide an important test for the accuracy of ozone-NO_x-ROG sensitivity as predicted by individual applications of urban models. The success of $O_3/(NO_y - NO_x)$ as an indicator is especially important as a tool for model evaluation. At present, regulatory decisions in the United States are made on the basis of results of photochemical models that are evaluated in terms of their ability to simulate measured O_3. The results of this paper suggest that evaluation of model performances in comparison with measured peak O_3 and concurrent $NO_y - NO_x$ would provide a stronger basis for confidence in predicted NO_x-ROG sensitivity.

Appendix: Derivation of O_3-ROG-NO_x Sensitivity in Terms of ROG/NO_x, H_2O_2/HNO_3, and O_3/NO_y Ratios

The split between ROG-sensitive and NO_x-sensitive photochemistry can be derived in theory from the steady state equation for odd hydrogen radicals (equation (1)). Production of O_3 is assumed equal to the summed rates of the OH + RH and OH + CO reactions (R1) and (R4). In addition, equation (1) will be modified to include formation of organic nitrates (including both PAN and alkyl nitrates) as a sink for odd hydrogen with the assumption that the rate of formation (P_{PAN}) is directly proportional to production rate for O_3. By using the following nomenclature substitutions,

$$P_{O_3} = k_4[CO][OH] + k_1[RH][OH] \quad \text{(A1a)}$$

$$f_{PAN} = \frac{P_{PAN}}{P_{O_3}} \quad \text{(A1b)}$$

$$\chi = \frac{k_1[RH]}{k_4[CO] + k_1[RH]} \quad \text{(A1c)}$$

$$\psi_1 = \frac{[NO]}{[NO_x]} \qquad \psi_2 = \frac{[NO_2]}{[NO_x]} \quad \text{(A1d)}$$

$$k_{56} = \frac{k_5}{\psi_1^2 k_3^2} + \frac{k_6\chi}{\psi_1^2 k_2 k_3} \quad \text{(A1e)}$$

Equation (1) becomes

$$S_H = \frac{\chi k_7 \psi_2 [NO_x]}{k_1[RH]} P_{O_3} + k_{56}\frac{1}{[NO_x]^2} P_{O_3}^2 + P_{PAN} \quad \text{(A2)}$$

The transition between the NO_x- and ROG-sensitive regimes can be identified by equating partial derivatives for P_{O_3} with respect to a percentage increase in NO_x ($\partial NO_x/NO_x$) or RH ($\partial RH/RH$):

$$[RH]\frac{\partial P_{O_3}}{\partial [RH]} = [NO_x]\frac{\partial P_{O_3}}{\partial [NO_x]} \quad \text{(A3)}$$

Equation (A3) will be substituted into (A2) with the assumption that both S_H and P_{PAN} can be expressed as functions of P_{O_3}; i.e., $\frac{\partial}{\partial [RH]}$ and $\frac{\partial}{\partial [NO_x]}$ are zero for these terms. The analytical relation between PAN and O_3 is discussed by *Sillman et al.* [1990b, 1991]. It will also be assumed that χ is constant. The resulting substitution yields

$$P_{O_3} = \frac{\chi k_7 \psi_2}{k_1 k_{56}} \frac{[NO_x]^3}{[RH]} \quad \text{(A4)}$$

Equation (A4) can be substituted into the rate expressions for reactions (R5), (R6), and (R7) to obtain a criterion for the transition point between NO_x-sensitive and ROG-sensitive chemistry in terms of photochemical production rates for H_2O_2, ROOH, and HNO_3 ($P_{H_2O_2}$, P_{ROOH}, and P_{HNO_3}):

$$P_{HNO_3} = 2(P_{H_2O_2} + P_{ROOH}) \quad \text{(A5)}$$

Equation (A5) provides the rationale for the use of peroxide to nitric acid ratios as indicators for sensitivity with an apparent transition point at $(H_2O_2 + ROOH)/HNO_3 = 0.5$, where ROOH is assumed to represent organic peroxides formed via reaction (R6) only. This is equivalent to a transition point at $H_2O_2/HNO_3 = 0.35$ based on the relative magnitude of reactions (R5) and (R6) in the simulations. The simulation results in Table 1 show transition points at $H_2O_2/HNO_3 \equiv 0.3$-0.6 with the highest transition ratios in simulations with greatest photochemical aging. The higher transition ratios in aged air may be caused by the higher rate of dry deposition of HNO_3 relative to H_2O_2.

Equation (A5) can also be used to obtain transition criteria in terms of O_3, NO_y, and NO_x. Substitution of (A5) into (A2) yields

$$S_H = 2P_{HNO_3} + P_{PAN} \quad \text{(A6)}$$

Sources of odd hydrogen (S_H) include photolysis of both O_3 and aldehydes, where aldehyde concentrations tend to increase with increasing O_3. If it is assumed that the source of odd hydrogen is proportional to O_3, then the transition between NO_x- and ROG-sensitive chemistry should be associated with a fixed value for the ratio

$$\frac{O_3}{NO_y - NO_x + HNO_3} \quad \text{(A7)}$$

In practical terms this suggests the use of either $O_3/(NO_y - NO_x)$ or O_3/HNO_3 as an indicator for NO_x-ROG sensitivity.

The use of the slope of O_3 versus $NO_y - NO_x$ as an indicator can also be justified by converting (A2) to differential form,

$$\Delta S_H = \Delta(2P_{H_2O_2} + 2P_{ROOH} + P_{HNO_3} + P_{PAN}) \quad \text{(A8)}$$

where ΔS_H versus $\Delta(P_{HNO_3} + P_{PAN})$ can be associated with the slope of O_3 versus $NO_y - NO_x$ for an ensemble of measurements. In combination with the criteria defined by (A5), this suggests that an ensemble of points with ROG-sensitive chemistry (with

high $P_{HNO_3}/P_{H_2O_2}$) will have a lower $\Delta O_3/\Delta(NO_y - NO_x)$ than a NO_x-sensitive ensemble with low $P_{HNO_3}/P_{H_2O_2}$. However, a low $\Delta O_3/\Delta(NO_y - NO_x)$ can also be indicative of an ensemble of points in transition between NO_x- and ROG-sensitive chemistry (with rapidly varying $P_{HNO_3}/P_{H_2O_2}$) as well as an ROG-sensitive ensemble.

A link between NO_x-ROG sensitivity and the ratio ROG/NO_x can also be derived from equations (A2) and (A4) if it is assumed that the odd hydrogen source term increases with P_{O_3}. In this case, (A2) and (A4) combine to yield the following criterion for the transition from NO_x- to ROG-sensitive chemistry:

$$\frac{k_1[RH]}{[NO_x]} = \frac{2\chi k_7 \psi_2}{\partial S_H / \partial P_{O_3}} \quad \text{(A9)}$$

This is the familiar result that the transition between NO_x-sensitive and ROG-sensitive O_3 in polluted environments occurs at a fixed ROG/NO_x ratio, with a higher ratio corresponding to NO_x-sensitive O_3. The requisite assumption ($S_H \sim P_{O_3}$) is valid only in the limiting case of high RH and NO_x. The product $k_1[RH]$ in (A9) implicitly represents a reactivity-weighted sum of ROG because $k_1[RH]$ represents the the sum of many individual RH + OH reactions [see *Chameides et al.*, 1992].

It is useful to compare this formulation of NO_x- and ROG-sensitive photochemistry with the NO_x- and radical-limited regimes of *Kleinman* [1991, 1994]. Kleinman's radical-limited regime represents a situation in which the source term for odd hydrogen (S_H) is smaller than the NO_x source (S_N), i.e., $S_H < S_N$, and is characterized by continually increasing NO_x, very low OH, and no sigifnicant photochemical production of O_3. Sources and sinks for NO_x are in equilibrium in Kleinman's calculation ($S_N = P_{HNO_3} + P_{RN}$) unless $S_H > S_N$. In these terms, ROG-sensitive chemistry is associated with the criteria (from (A6))

$$S_H < \xi S_N \quad \text{(A10a)}$$

$$\xi = 1 + \frac{P_{HNO_3}}{P_{HNO_3} + P_{RN}} \quad \text{(A10b)}$$

The region where $S_N < S_H < \xi S_N$ is of special interest for urban photochemistry, because it includes significant OH-driven chemistry and production of O_3 but the rate of ozone production is sensitive to ROG rather than to NO_x. True NO_x-sensitive chemistry only occurs when $S_H > \xi S_N$. The inclusion of NO_x- and ROG-sensitive regimes as defined here appears to represent a significant addition to Kleinman's formulation. The NO_x- and ROG-sensitive regime defined here are also associated with the multiple steady state solution hypothesized by *Kleinman* [1994].

Acknowledgements. Discussions with Jana Milford, William Chameides and Peter Daum were especially helpful in preparing this manuscript. Bart Croes, Robert Imhoff, Jai-Hon Lee, and Daniel Jacob provided timely access to measurements. This work was supported by the United States Environmental Protection Agency, Atmospheric Research and Exposure Assessment Laboratory (AREAL) grant CR 822083-01-0 and by the Southern Oxidant Study. The contents of this paper do not necessarily reflect the views of the United States Environmental Protection Agency.

References

Blanchard, C., P. M. Roth, and H. E. Jeffries, Spatial mapping of preferred strategies for reducing ambient ozone concentrations nationwide, paper presented at 86th Annual Meeting and Exposition, Air and Waste Manage. Assoc., Denver, Colo., June 13-18, 1993.

Chameides, W. L., et al., Ozone precursor relationships in the ambient atmosphere, *J. Geophys. Res.*, 97, 6037-6056, 1992.

DeMore, W. B., S. P. Sander, D. M. Golden, R. F. Hampson, M. J. Kurylo, C. J. Howard, A. R. Ravishankara, C. E. Kolb, and M. J. Molina, Chemical kinetics and photochemical data for use in stratospheric modeling, *Rep. JPL 92-20*, Jet Propul. Lab., Pasadena, Calif., 1992.

Environmental Protection Agency, Development of the 1980 NAPAP emissions inventory, *Rep. EPA-600/7-86-057a*, Research Triangle Park, N. C., 1986.

Fehsenfeld, F. C., et al., A ground-based intercomparison of NO, NO_x, and NO_y measurement techniques, *J. Geophys. Res., 92;* 14,710-14,722, 1987.

Flowers, E. C., R. A. McCormick, and K. R. Kurfis, Atmospheric turbidity over the United States, 1961-1966, *J. Appl. Meteorol., 8,* 955-962, 1969.

Fujita, E. M., B. E. Croes, C. L. Bennett, D. R. Lawson, F. W. Lurmann, and H. H. Main, Comparison of emission and ambient concentration ratios of CO, NO_x, and NMOG in California's south coast air basin, *J. Air Waste Manage. Assoc., 42;* 264-276, 1992.

Geron, C. D., A. B. Guenther, and T. E. Pierce, An improved model for estimating emissions of volatile organic compounds from forests in the eastern United States. *J. Geophys. Res., 99,* 12,773-12,791, 1994.

Hering, S.V., et al., The nitric acid shootout: Field comparison of measurement methods, *Atmos. Environ, 22;* 1519-1539, 1988.

Jacob, D. J., L. W. Horowitz, J. W. Munger, B. G. Heikes, R. R. Dickerson, R. S. Artz, and W. C. Keene, Seasonal transition from NO_x- to hydrocarbon-limited ozone production over the eastern United States in September, *J. Geophys. Res.*, in press, 1995.

Jacob, D. J., and S. C. Wofsy, Photochemistry of biogenic emissions over the Amazon forest, *J. Geophys. Res., 93,* 1477-1486, 1988.

Johnson, G. M., A simple model for predicting the ozone concentration of ambient air, Proceedings, *Eighth International Clean Air Conference*, Melbourne, Australia, Volume 2, p. 715-731. Eds. H. F. Hartmann, J. N. O'Heare, J. Chiodo, and R. Gillis. (Clean Air Society of Australia and New Zealand) 1984.

Johnson, G. M., S. M. Quigley, and J. G. Smith. Management of photochemical smog using the AIRTRAK approach paper presented at 10th International Conference, Clean Air Soc. of Australia and New Zealand, Aukland, New Zealand, March 1990.

Kleindienst, T. E., et al., An intercomparison of formaldehyde measurement techniques at ambient concentration, *Atmos. Environ., 22;* 1931-1940, 1988.

Kleinman, L. I., Photochemical formation of peroxides in the boundary layer, *J. Geophys. Res., 91,* 10,889-10,904, 1986.

Kleinman, L. I., Seasonal dependence of boundary layer peroxide concentration: The low- and high-NO_x regimes, *J. Geophys. Res., 96,* 20,721-20,734, 1991.

Kleinman, L. I., Low- and high-NO_x tropospheric photochemistry, *J. Geophys. Res., 99,* 16,831-16,838, 1994.

Lamb, B., H. Westberg, G. Allwine, and T. Quarles, Biogenic hydrocarbon emissions from deciduous and coniferous trees in the United States, *J. Geophys. Res., 90,* 2380-2390, 1985.

Lee, J. H., D. F. Leehy, I. N. Tang, and L. Newman, Measurement and speciation of gas phase peroxides in the atmospher, *J. Geophys. Res., 98,* 2911-2915, 1993.

Lee, J. H., I. N. Tang, J. B. Weinstein-Lloyd, and E. B. Halper, An improved nonenzymatic method for the determination of gas-phase peroxide, *Environ. Sci. Technol., 28,* 1180-1185, 1994.

Lin, H., M. Trainer, and S. C. Liu, On the nonlinearity of tropospheric ozone, *J. Geophys. Res., 93,* 15,879-15,888, 1988.

Liu, S. C., M. Trainer, F. C. Fehsenfeld, D. D. Parrish, E. J. Williams, D. W. Fahey, G. Hubler, and P. C. Murphy, Ozone production in the rural troposphere and implications for regional and global ozone distributions. *J. Geophyus. Res., 92,* 4191-4207, 1987.

Logan, J. A., Tropospheric ozone: Seasonal behavior, trends, and anthropogenic influence, *J. Geophys. Res., 90,* 10,463-10,482, 1985.

Lurmann, F. W., A. C. Lloyd, and R. Atkinson, A chemical mechanism for use in long-range transport/acid deposition computer modeling, *J. Geophys. Res. 91*, 10,905-10,936, 1986.

Madronich, S., Photodissociation in the atmosphere; 1, Actinic flux and the effect of ground reflections and clouds, *J. Geophys. Res. 92*, 9740-9752, 1987.

Matthews, E., Global vegetation and land use: New high-resolution data bases for climate studies, *J. Clim. Appl. Meteorol.*, 22, 474-487, 1983.

McKeen, S. A., E.-Y. Hsie, and S. C. Liu, A study of the dependence of rural ozone on ozone precursors in the eastern United State, *J. Geophys. Res.*, *96*, 15,377-15,394, 1991.

Milford, J., A. G. Russell, and G. J. McRae, A new approach to photochemical pollution control: Implications of spatial patterns in pollutant responses to reductions in nitrogen oxides and reactive organic gas emission, *Environ. Sci. Technol.*, *23*, 1290-1301, 1989.

Milford, J., Y.-J. Yang, and W. R. Stockwell, Uncertainties in chemical mechanisms for urban and regional-scale oxidant modeling, paper presented at International Conference on Regional Photochemical Modeling and Measurement, Air and Waste Manage. Assoc., San Diego, Calif., Nov. 8-12, 1993.

Milford, J., D. Gao, S. Sillman, P. Blossey, and A. G. Russell, Total reactive nitrogen (NO_y) as an indicator for the sensitivity of ozone to NO_x and hydrocarbons, *J. Geophys. Res.*, *99*, 3533-3542, 1994.

National Research Council Committee on Tropospheric Ozone Formation and Measurement, *Rethinking the Ozone Problem in Urban and Regional Air Pollution*, National Academy Press, Washington, D.C., 1991.

Paulson, S. E., and J. H. Seinfeld, Development and evaluation of a photooxidation mechanism for isoprene, *J. Geophys. Res.*, *97*, 20,703-20,715, 1992.

Possiel, N. C., L. B. Milich, and B. R. Goodrich (Eds.), Regional qzone modeling for northeast transport (ROMNET), *Rep. EPA-450/4-91-002a*, U.S. Environ. Pro. Agency, Research Triangle Park, N. C., July 1991.

Sillman, S., A numerical solution to the equations of tropospheric chemistry based on an analysis of sources and sinks of odd hydrogen, *J. Geophys. Res.*, *96*, 20,735-20,744, 1991.

Sillman, S., J. A. Logan, and S. C. Wofsy, A regional-scale model for ozone in the United States with a sub-grid representation of urban and power plant plumes, *J. Geophys. Res*, *95*, 5731-5748, 1990a.

Sillman, S., J. A. Logan, J. A. and S. C. Wofsy, The sensitivity of ozone to nitrogen oxides and hydrocarbons in regional ozone episodes. *J. Geophys. Res.*, *95*, 1837-1851, 1990b.

Sillman, S., P. J. Samson, and J. M. Masters, Ozone production in urban plumes transported over water: Photochemical model and case studies in the northeastern and midwestern United States, *J. Geophys. Res.*, *98*, 12,687-12,699, 1993.

Sillman, S., et al., Photochemistry of ozone formation in Atlanta, GA: Models and measurements; *Atmos. Environ.*, in press, 1995.

Tesche, T. W., P. Georgeopoulos, J. H. Seinfeld, G. Cass, F. L. Lurmann and P. M. Roth, Improvement of procedures for evaluating photochemical models. Report prepared by Radian Corporation, State of Calif. Air Resour. Board, Sacramento, Calif., 1990.

Trainer, M., et al., Correlation of ozone with NO_y in photochemically aged air, *J. Geophys. Res.*, *98*, 2917-2926, 1993.

S. Sillman, Department of Atmospheric, Oceanic, and Space Sciences, Space Physics Research Lab, University of Michigan, Ann Arbor, MI 48109. (e-mail: Sillman@umich.edu)

(Received February 3, 1994; revised September 21, 1994; accepted October 5, 1994).